Evolution of hydrogen and helium co-implanted single-crystal silicon during annealing

Xinzhong Duo,[a] Weili Liu, Miao Zhang, Lianwei Wang, and Chenglu Lin
Shanghai Institute of Metallurgy, Chinese Academy of Sciences, Shanghai 200050, People's Republic of China

M. Okuyama and M. Noda
Area of Materials and Device Physics, Department of Physical Science, Graduate School of Engineering Science, Osaka University, 1-3 Machikaneyama-cho, Toyanaka, Osaka 560-8531, Japan

Wing-Yiu Cheung and S. P. Wong
Department of EEE, Chinese University of Hong Kong, New Territory, Hong Kong, People's Republic of China

Paul K. Chu
City University of Hong Kong, Tat Chee Avenue, Kowloon, Hong Kong, People's Republic of China

Peigang Hu
Applied Ion Beam Physics Laboratory, Fudan University, Shanghai, 200433, People's Republic of China

S. X. Wang and L. M. Wang
Department of Nuclear Engineering and Radiological Sciences, College of Engineering, The University of Michigan, Ann Arbor, Michigan 48109-2104

(Received 14 November 2000; accepted for publication 6 June 2001)

H^+ was implanted into single-crystal silicon with a dose of $1\times10^{16}/cm^2$ and an energy of 30 KeV, and then He^+ was implanted into the same sample with the same dose and an energy of 33 KeV. Both of the implantations were performed at room temperature. Subsequently, the samples were annealed in a temperature range from 200 to 450 °C for 1 h. Cross-sectional transmission electron microscopy, Rutherford backscattering spectrometry/channeling, elastic recoil detection, and high resolution x-ray diffraction were employed to characterize the strain, defects, and the distribution of H and He in the samples. The results showed that co-implantation of H and He decreases the total implantation dose, with which the surface could exfoliate during annealing. During annealing, the distribution of hydrogen did not change, but helium moved deeper and its distribution became sharper. At the same time, the maximum of the strain in the samples decreased a lot and also moved deeper. Furthermore, the defects introduced by ion implantation and annealing were characterized by slow positron annihilation spectroscopy, and two positron trap peaks were found. After annealing, the maximum of these two peaks decreased at the same time and their positions moved towards the surface. No bubbles or voids but cracks and platelets were observed by cross-sectional transmission electron microscopy. Finally, the relationship between the total implantation dose and the fraction of hydrogen in total implantation dose was calculated. [DOI: 10.1063/1.1389478]

I. INTRODUCTION

Hydrogen profoundly alters the electrical characteristics of the resultant device by diffusing into active region and passivating the dopant.[1–3,4] Both of hydrogen and helium implantation could cause surface exfoliation and blistering under similar conditions.[4–7] Furthermore, the voids introduced by H^+ or He^+ implantations have been demonstrated as efficient gettering centers of transition metal impurities. Presently, great interest has been focused on the smart-cut process (one of the most important steps in Unibond silicon-on-insulator (SOI) materials fabrication), which is based on the observation of exfoliation and blistering caused by implantation of hydrogen or helium.[8] This process allows SOI wafers to be fabricated more economically and with better quality than the competing processes such as SIMOX (separated by implantation oxygen) and BESOI (bonded and etch-back SOI). Gas ion implantation, usually hydrogen, is a necessary step in the smart-cut process. The thin film separation process is based on the observation that implantation of a high dose of hydrogen induces blistering and exfoliation on the surface of metal and semiconductor. Generally, it is considered that the thin film separation process is proceeded by chemical interaction (bond breaking and internal surface passivation) and physical interaction (gas coalescence, pressure, and fracture) of implanted H^+ in the silicon substrate. It is difficult to isolate the contribution of each component to the overall process. Helium is another kind of gas used in thin film separation. Helium does not proceed chemical interaction in silicon substrate as hydrogen, but it proceeds physical

[a]Electronic mail: duoxz@yahoo.com

interaction just as hydrogen does and even more efficiently.[9] Co-implantation of hydrogen and helium is a good way to study the different role of the implanted gas ion in the smart-cut process,[10] the interaction between the two kinds of atoms, and the correlation between the defects of the H/He atoms. It helps to decouple the physical and chemical contributions in the blistering and thin film separation processes. Co-implantation needs much lower total dose of ion implantation than that of H or He implanted alone. It shortens the implantation time and decreases crystal damage induced by implantation. As a result, the cost of SOI fabrication decreases and the quality of SOI material improves.

In this work, high resolution x-ray diffractometer (HRXRD), Rutherford backscattering spectrometry and channeling (RBS/C), elastic recoil detect analysis (ERDA), Cross-sectional transmission electron microscope (XTEM) and slow position annihilation spectroscopy (SPAS) were employed to study the co-implanted samples annealed at different temperatures.

II. EXPERIMENT

P-type (5–8 Ω cm) (100) silicon wafers were implanted with H^+ at an energy of 30 KeV and a dose of $1\times10^{16}/cm^2$, then He^+ at an energy of 33 KeV and a dose of $1\times10^{16}/cm^2$ at room temperature. In order to avoid the channeling effects, deliberate misalignment from the wafer normal of 7° was performed during implantation. After implantation, all wafers were cut into smaller samples for analysis. The samples were given a standard reduced calcium aluminate clean prior analysis to remove surface contaminants introduced by the implantation and then were annealed in the temperature range 200–450 °C for 1 h in the flowing ambient of N_2 gas. The implanted samples were then stored in air at room temperature before measurement.

HRXRD was performed by Philips X pert equipped with a two crystal Ge [220] diffractometer. The Cu $K\alpha_1$ radiation with the wavelength 1.5406 Å was used in all the experiments. Scans of $\omega/2\theta$ scans were performed on (004) of the samples. Interstitial atoms and defects bring strain due to their volume and static disorder. This technique is very sensitive to the lattice displacement and strain in the direction perpendicular to the working diffraction plane of the crystal. The curves were computer simulated and, as a result, the profiles of the perpendicular component to the surface of the strain ϵ were obtained.

RBS/C was performed with 2.0 MeV He^+ ion beams. The scattering angle of the RBS spectrum was 140°. In this technique, the backscattering yield is sensitive to the defects in the crystalline matrix. The signal is produced by the silicon atoms unaligned to the channel rows, in our case, the atoms displaced from their crystalline position in the directions parallel to the surface, especially the interstitial silicon atoms. Rather than the raw RBS data, the profiles of displacement atoms were calculated according to the algorithm developed in Ref. 11. In the following, we shall consider the displacement atom profile as a quantity proportional to the intensity of the displacement field. HRXRD and RBS/C can be considered as complementary techniques in detecting the three-dimensional displacement field caused by point-like defects.

XTEM samples (annealed at 450 °C for 1 h) were prepared in the conventional way by mechanical thinning and Ar^+ ion etching. XTEM observation was concerned with distribution and location of extended defects, bubbles, and platelets.

The H and He distributions in Si samples after implantation and annealing were measured by ERDA, using a 12 MeV $^{16}O^{4+}$ beam (with a cross section of 1×0.3 mm^2) impinging the sample at 75° from the sample normal. The detector was placed at 150° from the beam direction and the forward-scattered oxygen particles were stopped by a 10-μm-thick Mylar film. The RUMP program was used to analyze the raw data and calculate the depths and the concentrations of both components.

The profiles of vacancy-type defects were characterized by slow positron beam. The SPAS is highly sensitive to open volume defects for the positron is apt to be trapped and annihilated in sites where the Coulomb core repulsion is a minimum.[12] The positrons were implanted in an energy range from 0.5 to 15 KeV. The Doppler broadening of the 511 KeV annihilation γ rays was measured at room temperature. The mean depth z(nm) of the incident positron is given by $z=(A/\rho)E^n$, where E(KeV) is the incident positron energy and ρ(g·cm^{-3}) is the mass density of the target. For Si target, the constants A and n are empirically determined to be 4.0 (μg cm^{-2} KeV^{-n}) and 1.6, respectively. The level of Doppler broadening is indicated by the S parameter, which is defined as the ratio of the counts in a fixed central region ($|511-E\gamma|<0.85$ KeV) of the 511 KeV line to the total counts of the peak ($|511-E\gamma|<4.25$ KeV). It should be stressed that vacancy-like defects are active positron traps if they are helium and hydrogen free, however once they are decorated by helium and hydrogen, they become ineffective in trapping positrons. The decrease of SPAS signal can be due either to the decrease of trap density in annealing or to the passivation by gases. Conversely, the rise of the SPAS signal can be due to depassivated traps resulting from helium and hydrogen outflow.

III. RESULTS

Ion implantation caused lattice swelling in the implantation region. And lattice swelling introduced strain near the surface of the samples. Rocking curves were computer simulated and, as a result, the distribution of strain was obtained. Because the light gas ion implantation creates slight damage in the samples and the low annealing temperature does not introduce much defect either, the Debye–Waller factor is neglected in the simulation of low temperature annealed samples. Strain distribution versus depth is shown in Fig. 1. However, when the samples were annealed at higher temperature, the implanted region became amorphous and the Debye–Waller factor's affection on rocking curves could not be neglected. Consequently, a unique determination of the local strain is impossible. So the rocking curves of samples annealed at temperature higher than 300 °C were not computer simulated. In Fig. 1 we can see that, after annealing at

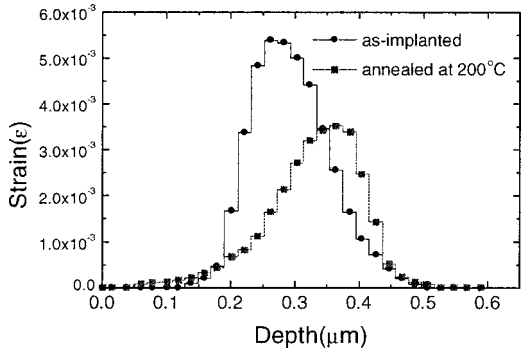

FIG. 1. The distribution of strain in the samples annealed at 200 °C and as-implanted samples. The distribution moves deeper after annealing, and becomes weaker and wider. From the rocking curves (not shown here), it is clear that the magnitude of the strain decreases more when annealed at 350 and 450 °C.

200 °C for 1 h, the magnitude of the strain decreased from 5.5×10^{-3} to 3.5×10^{-3}, and the maximum of the strain moved even deeper, from 300 to 400 nm. And the strain region became wider after annealing. Although data of samples annealed over 300 °C cannot be simulated, it is clear that the strain went on decreasing when the annealing temperature increased.

To characterize the distributions and the losses of hydrogen and helium during annealing, ERDA was employed. The distributions of hydrogen and helium are reported in Figs. 2(a) and 2(b), respectively. Hydrogen lost continuously as annealing temperature increased, especially when annealing temperature was 450 °C, at which samples exfoliated on the surface. But the total amount of helium did not change until the annealing temperature was up to 450 °C. The distribution of hydrogen does not change during annealing below 200 °C, and moves slightly deeper when annealed at 350 °C; while helium accumulated much sharper, and moved from the depth of 300 to 400 nm when annealing temperature was over 350 °C. The maximum of helium after annealing was almost equal to that of hydrogen. The density peaks of hydrogen around channel 330 are due to surface contamination. The implantation process was simulated by TRIM96.

During annealing in the temperature range from 200 to 450 °C, the density of the scattering center in the implanted region increased greatly. The damage in the wafers was investigated by RBS/C. The channeling spectra of the samples indicate the density of the displacement atoms. When the samples were annealed at 450 °C, the surface was blistered and exfoliated. RBS/C was invalidated in such a situation. A method described in Ref. 2 was used to analyze the RBS/C data and characterize the distribution of displacement atoms. The density of displacement atoms versus depth is presented in Fig. 3. The maximum of displacement atom density moved deeper with the increase of annealing temperature, especially in the temperature range from 200 to 350 °C. The displacement atoms distributed around the depth of 400 nm. It is clear that there were two density peaks of displacement atoms before annealing, and both of the peaks become wider and combined together during annealing.

XTEM was employed to show the distribution of defects, strain, platelets, and bubbles in the samples. In Fig. 4,

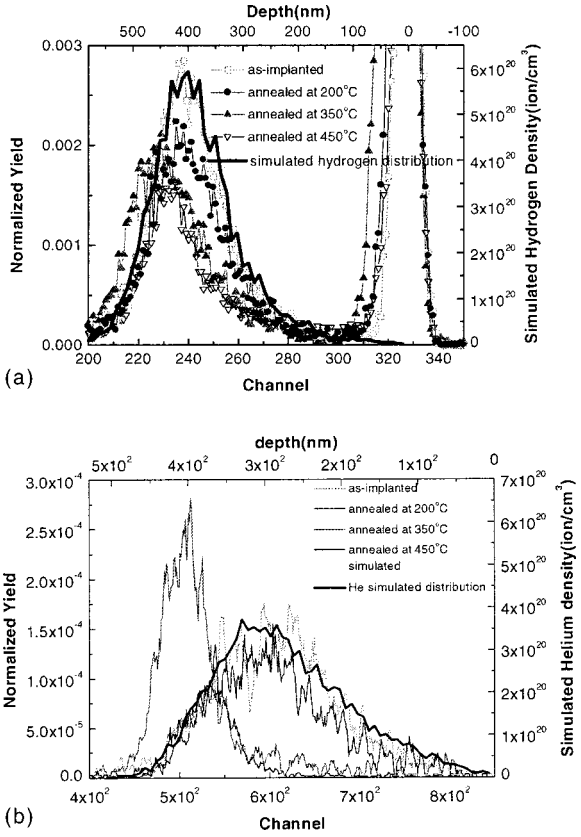

FIG. 2. ERDA yield for samples annealed at different temperature. (a) Distribution of hydrogen. The peak around channel 330 is the contamination on the surface. The density of hydrogen decreases with the annealing temperature. But the distributions keep the same below 450 °C. (b) Distribution of helium; it is very clear that after being annealed at 350 °C, the helium moves deeper and sharper.

a typical electron microscopy of a thinner section reveals that most of the platelets in the defect layer oriented along the (100) planes, while in crystal silicon implanted only by hydrogen, the majority of the platelets oriented along the (111) planes.[1] There were lots of dislocation and strain distributed near the projected range, which were induced by stress in the region. It is clear that there were few bubbles near the projected range in the co-implanted samples, while there were

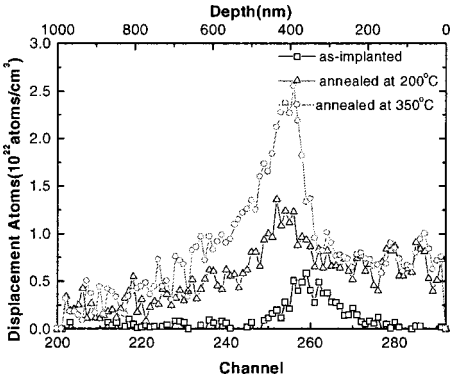

FIG. 3. Displacement atoms density vs depth in samples annealed at different temperature. The density of displacement atoms increases from a density of 0.5×10^{22} to 2.5×10^{22} with the increase of annealing temperature; and the distribution moves from a depth of 300 to 400 nm.

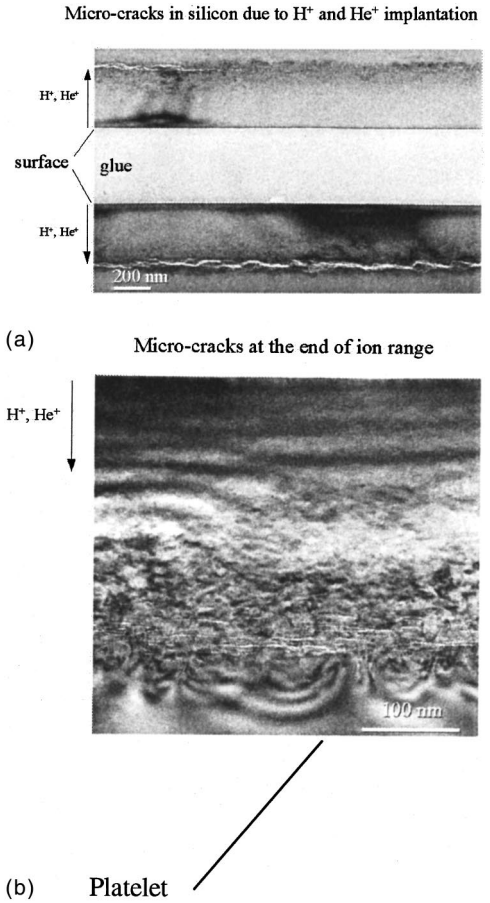

FIG. 4. XTEM image of the sample annealed at 450 °C. (a) The depth of the crack is about 400 nm. This should be the result of enlarged platelets connecting to each other. (b) Most of the platelets are oriented along {100} plane. These platelets have not connected to each other yet, great strain is distributed near the platelet region. No bubbles can be found in both figures.

much more bubbles in the hydrogen or helium alone implanted samples. The defects region was quite wide. It ranged from a depth from 200 to 400 nm. And the projected range of hydrogen in this experiment was about 400 nm.

The parameter S for SPAS analysis was low on the surface, because positrons diffused back to the surface. At high implantation energy, most positrons were deep enough to be annihilated far away from the defected region and in all the samples the S value reached the same asymptotic defect-free value of the material. In the defect region, the S value was higher than that in virgin silicon. This difference indicated that an increasing fraction of positrons annihilated with low momentum electrons and a characteristic of positrons trapped in open volume defects.

As discussed in Ref. 13, the physical information about the positron traps was well described by the difference of the S parameter of the defected sample minus the corresponding value of the reference sample

$$\Delta S = \frac{S - S_s}{S_d - S_b} - \frac{S_b - S_s}{S_d - S_b}\left[\frac{S - S_s}{S_b - S_s}\right]_{\text{VirginSi}}.$$

S_s is the value of S parameter in the surface layer, S_b is the value of the S parameter in undamaged bulk material, S_d is the value of S parameter in the damaged region. The ΔS versus depth is shown in Fig. 5. Based on the analysis, it is very clear that there were two density peaks of positron trap, one was at 200 nm, and the other was at 400 nm. After annealing at 400 °C for 1 h, the deeper peak was almost eliminated and the leftover of the peak moved to 300 nm, and the shallower peak became much weaker, too, and moved towards the surface to about 150 nm. It seems that both of the peaks became wider after annealing.

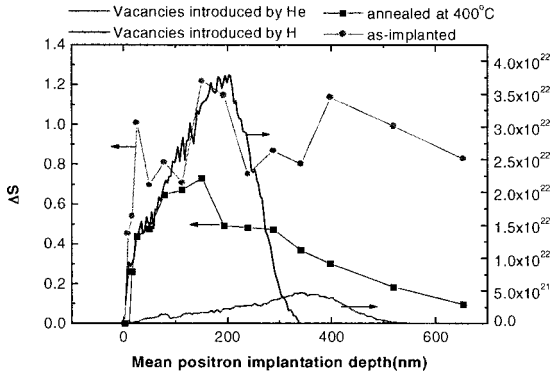

FIG. 5. ΔS vs mean positron implantation depth for samples annealed at 400 °C and as-implanted samples. ΔS indicates the density of positron traps in silicon wafers. There are two positron trap peaks in the samples. The deeper one should be introduced by hydrogen, and the shallower one should be introduced by helium. The distribution of positron traps moves towards the surface and the density of positron trapps decreases greatly after annealing.

IV. DISCUSSION

The experiment results can be summarized as follows.

(1) The total implantation dose that helium and hydrogen co-implantation needed to exfoliate the wafer's surface was lower than the dose that helium or hydrogen single implantation needed. ($>4\times10^{16}/\text{cm}^2$ hydrogen only, $>2\times10^{17}/\text{cm}^2$ helium only).
(2) Helium moved from its projected range to the hydrogen's projected range during annealing, while some of hydrogen escaped; the left hydrogen didn't change its position.
(3) The RBS/C profiles, the signature of silicon interstitial-like defects, increased with the annealing temperature.
(4) According to the computer simulated HRXRD result, the maximum of the strain moved deeper and decreased with the annealing temperature.
(5) The SPAS profiles, the signature of vacancy-like defects that are not fully saturated, decreased in density during annealing.
(6) Helium atoms, strain, and displacement atoms moved deeper, and hydrogen atoms and the positron traps moved towards the surface. (When hydrogen was implanted alone, hydrogen atoms moved towards the surface, the strain and displacement atoms moved deeper; when helium was implanted alone, helium atoms and the strain moved towards the surface, the positron traps moved deeper).[12,14,15]

Hydrogen is a very active element. During implantation,

a large part of the implanted hydrogen ions react with the silicon atoms, dangling bonds or defects, and diverse kinds of the H-related complexes are formed near the projected range. Under some conditions (e.g., high temperature annealing), hydrogen atoms escape from the H-related complexes and combine with each other into hydrogen molecular. Hydrogen atom's diffusivity is very high in silicon even at room temperature. But most of the hydrogen is combined in the complexes, and cannot move. H_2 molecules are difficult to move in silicon lattice, too.

Helium is an inert element. During implantation, helium atoms do not react with the silicon atoms, dangle bonds, or defects. The implanted helium atoms stay near the projected range. Helium atom's diffusivity is much lower than that of hydrogen atom in a silicon wafer; it can hardly move in room temperature. But in a higher temperature, it is also movable.

Because hydrogen and helium react in silicon wafer differently during implantation and annealing, the defects introduced by them are also different. Hydrogen generally introduces vacancies, interstitial atoms, bubbles and cracks, platelets, while helium introduces only vacancies, interstitial atoms, and bubbles.

Generally, for both hydrogen and helium atoms, if they stay in the lattice, the lattice will be enlarged, and strain is introduced into the lattice; if they stay in the defects or platelets or bubbles or cavities, they will not introduce strain into the lattice. When the implantation dose is not too high, we suppose that the magnitude of strain in the co-implanted region is a direct ratio to the density of hydrogen and helium in the lattice (not hydrogen and helium in platelets or bubbles)

$$\epsilon = \alpha n_{\mathrm{H},I} N_{\mathrm{H}} + \beta n_{\mathrm{He},I} N_{\mathrm{He}} \tag{1}$$

In the above equation, α and β are the strain parameter of hydrogen and helium, respectively, $n_{\mathrm{H},I}$ is the fraction of hydrogen in lattice, and $n_{\mathrm{He},I}$ is the fraction of helium in lattice. Both of the $n_{\mathrm{H},I}$ and $n_{\mathrm{He},I}$ are functions of annealing temperature and annealing time. N_{H} and N_{He} are density of hydrogen and helium, respectively.

In Fig. 1 we can see that after the samples were annealed at temperatures above 300 °C, strain in the lattice was nearly cut down a half, and the distribution of strain was deeper and wider. From Figs. 2(a) and 2(b), it is clear that the density and distribution of hydrogen kept almost the same in that region as those in the samples without annealing, while the helium distribution moved much deeper and became sharper. It is concluded that the helium diffused from the original position to the hydrogen's projected range through interstitial position, and caused the depth of strain distribution to move deeper. But the total mount of helium and hydrogen in the lattice decreased after annealing.

According to the simulation result of TRIM96, the density of vacancy induced by helium implantation was much heavier than that induced by hydrogen implantation. And the distribution of vacancy was always shallower than that of the implanted ion that induces the vacancy. The distribution of helium was between the vacancies induced by helium and hydrogen, respectively. During annealing at about 350 °C the helium moved much deeper. The helium density peak's depth is equal to that of hydrogen. We should ascribe the redistribution of helium to the defects in the hydrogen-distributed region. In the samples implanted only by helium, helium always moved towards the surface.[14] As stated above, the defects introduced by helium and hydrogen are different. During annealing, the helium atoms were movable and moved towards the hydrogen-implanted region where free energy was lower. These defects near hydrogen's projected range should be introduced only by hydrogen. We ascribe the defect to platelets induced by hydrogen and cracks. Therefore, although the projected ranges of the hydrogen and helium are different, H and He could accumulate together during annealing.

During implantation, vacancies and displacement atoms were generated near the projected region. Because hydrogen and helium were light atoms, the density of vacancies and displacement atoms was not too high. From Fig. 3, there were two displacement atom density peaks in the as-implanted samples (the two peaks combined together when annealed at high temperature); in Fig. 5 there were two positron trap density peaks in the as-implanted sample and the sample annealed at 400 °C. The shallower one was introduced by helium and the deeper one was introduced by hydrogen. The depth of the maximum of the displacement atom was similar to that of the positron traps, but the displacement atom and the positron traps evolved differently during annealing. With the increase of annealing temperature, the density of displacement atoms increased rapidly, while the density of positron traps decreased very much when annealing temperature was over 400 °C. Since a great mount of hydrogen and helium exist in the lattice after implantation, the interstitial gas atoms increased the free energy of the system, especially near the projected range. During annealing, more and more silicon atoms were kicked out to the interstitial position to decrease the free energy, and Frenkel pairs formed. Therefore the density of interstitial silicon atoms (one kind of displacement atoms) increased rapidly, which can be concluded from the result of RBS/C. During annealing, both of the gas atoms were movable. Because of the lower free energy in the vacancies, gas atoms accumulated there. Hydrogen combined with these vacancies and formed VH_n.[16] The vacancies were filled with the gas atoms and were passivated, so that the vacancies lost the ability to trap positron. Furthermore, helium atoms moved deeper, and vacancies in the region near surface were not fully passivated. So the maximum of positron trap moved towards the surface.

If there is enough hydrogen in the samples, the role of implanted H is twofold; first, it acts chemically so it drives the formation of microscopically flat internal surfaces—platelets—and acts as a source of gaseous H_2 which is traped in the internal cavities; second, it acts physically as an internal pressure source. Helium only acts physically as an internal pressure source. During hydrogen ion implantation, extended defects, platelets, and vacancies are introduced. Inner surfaces of these extended defects are hydronized. Some of the Si–Si bonds are replaced by Si–H–H–Si bonds (one of the most important H-related complexes that cause exfoliation) which are much weaker than Si–Si bonds.[1] During annealing, some of the H-related complex relapses, hydrogen atoms are released, and combine with each other. Therefore,

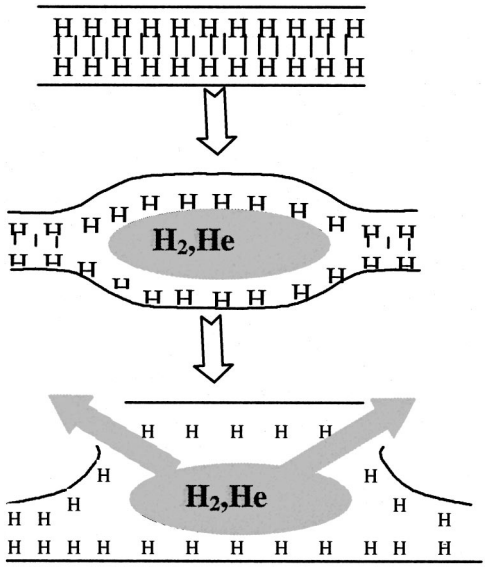

FIG. 6. The evolution process from H-related complex to platelets; (a) as-implanted, H-related complex forms; (b) platelets come into being, and gas accumulates in them during annealing, (c) surface exfoliates under the great gas pressure when annealed at high temperature.

hydrogen molecules are formed in silicon crystal. Break of hydrogen bond in Si–H–H–Si introduces platelets. During annealing at higher temperature, H_2 molecular and He atoms are movable. If the H_2 molecular and He atoms stay in the platelets, the free energy of the system is much lower than that when they stay in interstitial place or vacancies. So H_2 molecular and helium atoms are apt to accumulate in these extended defects, and exert great pressure on the inner surface of extended defects. The structure of platelet is easier to split than other extended defects (such as bobbles) due to their mechanical and chemical structure. During annealing, more and more H_2 molecular and helium atoms are released from lattice and accumulate in the platelets, The platelets become larger and larger under the inner pressure, finally some of them connect with each other as shown in Fig. 4(a). The diameter of the platelets is about several nanometers before annealing, and is about several tens of nanometers after annealing.[9] When annealing temperature is above 400 °C, blister and exfoliation occur. During the split process, platelets play a much more important role than the bubbles. The above processes are shown in Fig. 6. Helium plays an important role in that process. First, helium will not combine with the silicon atoms and move slowly, so during annealing at a certain temperature, it will neither escape nor be captured by defect, so that it is much easier for helium to accumulate in platelets than hydrogen; second, helium is single atom molecular, and it doubles the effect when implanted with the same dose as hydrogen. We should not worry whether the project ranges are exactly the same or not; it only requested that the difference of the projected ranges is within a certain range. According to our experiments, the difference of the projected range can be more than 200 nm.

Based on the model of exfoliation stated above, the relationship between hydrogen/helium total co-implantation dose and the fraction of hydrogen in implantation is calculated.

We divide all of the hydrogen and helium in silicon wafers into two forms, the component in lattice and the component in platelets. We suppose the average free energy of hydrogen in lattice is $E_{\mathrm{H},I}$, and the average free energy of hydrogen in platelet is $E_{\mathrm{H},P}$, the average free energy of helium in lattice is $E_{\mathrm{He},I}$, the average free energy of helium in platelet is $E_{\mathrm{He},P}$. D_{H} and D_{He} are the implantation dose of hydrogen and helium, respectively. The term ρ_s is the surface density of hydrogen atoms and $f(T)$ is the thermodynamic fraction which comes off the walls; γ is the surface energy of the wall in platelets and r_0 is the average diameter of a platelets. N_0 is the average number of gas molecules in a platelet. N_{platelet} is the density of platelets. $N_{\mathrm{H},P}$ and $N_{\mathrm{He},P}$ are the density of hydrogen and helium atoms in bubbles or platelets, respectively. $N_{\mathrm{H},I}$ and $N_{\mathrm{H},I}$ are the density of hydrogen and helium atoms in lattice; r_{ex} is the average radius of the platelets when they connect to each other during annealing. According to our experiment result, the temperature T_{ex}, at which the surface exfoliated during annealing, is almost the same in different implantation dose samples. We get the following formula:

$$N_{\mathrm{H},P}/N_{\mathrm{H},I}=e^{-E_{\mathrm{H},P}/k_BT}/e^{-E_{\mathrm{H},I}/k_BT}, \tag{2}$$

$$N_{\mathrm{He},P}/N_{\mathrm{He},I}=e^{-E_{\mathrm{He},P}/k_BT}/e^{-E_{\mathrm{He},I}/k_BT}. \tag{3}$$

Equations (2) and (3) are the relations between the numbers of gas atoms in different states under Boltzmann distribution

$$N_{\mathrm{platelet}}=CN_{\mathrm{H},I}, \tag{4}$$

$$r_0^2=\frac{1}{4\pi}\frac{3k_BTN_0}{\gamma-\frac{4}{3}\rho_s k_BTf(T)\ln\left(\frac{3TN_0}{4\pi\gamma}\right)}. \tag{5}$$

Equation (5) is cited from Ref. 17, as relation between the radius of platelets and the annealing temperature and the number of gas molecules in the platelet. To simplify the calculating, we suppose that all the platelets are in the same depth, and parallel to the surface

$$N_{\mathrm{platelet}}r_{\mathrm{ex}}^2=1, \tag{6}$$

$$N_0=(\tfrac{1}{2}N_{\mathrm{H},P}+N_{\mathrm{He},P})/N_{\mathrm{platelets}}. \tag{7}$$

Equation (6) is the condition when the platelets connect to each other; $r_0>r_{\mathrm{ex}}$ is the condition of exfoliation. Equation (7) is the average gas molecular number in one platelet.

We suppose that when $r_0>r_{\mathrm{ex}}$, the surface will exfoliate, Combining the former formula, we can see that

$$\frac{\alpha D_{\mathrm{H}}+\beta D_{\mathrm{He}}}{\gamma-\delta\ln[(\alpha D_{\mathrm{H}}+\beta D_{\mathrm{He}})/k_B\gamma N_{\mathrm{platelets}}^2]}\geqslant 1, \tag{8}$$

α, β, χ are constants derived from the formulas above.

$$\alpha=\frac{3k_BT_{ex}}{8\pi[1+\exp(E_{\mathrm{H},P}-E_{\mathrm{H},T})/k_BT_{\mathrm{ex}}N_{\mathrm{platelets}}]},$$

$$\beta=\frac{3k_BT_{ex}}{4\pi(1+\exp[(E_{\mathrm{H},P}-E_{\mathrm{H},T})/k_BT_{\mathrm{ex}}N_{\mathrm{platelets}}]},$$

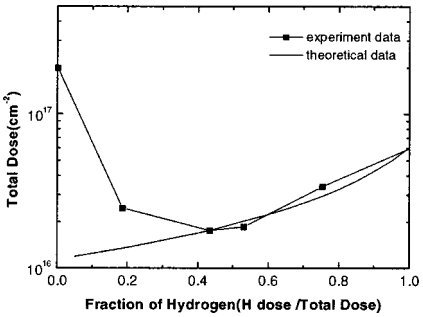

FIG. 7. The experiment data (in Ref. 17) and theoretical curve of the necessary co-implantation dose that is able to cause exfoliation on the sample surface. The theoretical curve fits the experiment data when hydrogen's implantation dose is high enough. When hydrogen is not implanted or is implanted with a very low dose, the minimum total dose that could cause exfoliation rises rapidly. This theory cannot explain such a situation when hydrogen is too few to introduce enough platelets in the samples.

$$\delta = \tfrac{4}{3}\rho_s k_B T_{\mathrm{ex}} f(T_{\mathrm{ex}}).$$

The radius of the platelets is quite small under the hypothesis above, according to Ref. 10, we can conclude that $\gamma \gg \delta \ln[(\alpha D_{\mathrm{H}} + \beta D_{\mathrm{He}})/k_B \gamma N^2_{\mathrm{platelets}}]$, we get

$$\alpha D_{\mathrm{H}} + \beta D_{\mathrm{He}} \geqslant \gamma. \tag{9}$$

Compared with the experiment data in Ref. 17, if implant hydrogen only, the minimum dose is $6\times10^{16}/\mathrm{cm}^2$, if hydrogen implantation dose is $0.75\times10^{16}/\mathrm{cm}^2$, the helium minimum implantation dose is about $1\times10^{16}/\mathrm{cm}^2$, and we get $\alpha/\gamma = 1.67\times10^{-17}/\mathrm{cm}^2$, $\beta/\gamma = 8.75\times10^{-17}/\mathrm{cm}^2$. The theoretic line fits the experiment data very well when the hydrogen implantation dose is not too low. The result is shown in Fig. 7.

When only helium ions are implanted or the content of hydrogen is very low, the situation is quite different. Because of the absence of platelets introduced by hydrogen, the surface exfoliation is caused only by the pressure in bubbles, which is much more difficult to cause exfoliation than platelets. It will not be discussed here.

V. CONCLUSION

Co-implantation of helium and hydrogen decrease the total dose to induce exfoliation. The reason why co-implantation could decrease the total implantation dose was explained. The evolution of defects in samples during annealing was analyzed. And it is found that helium moved from its projected range to that of hydrogen, it is unnecessary to make the projected range exactly the same during co-implantation. Furthermore, the relation between total implantation dose and the fraction of hydrogen in co-implantation was calculated.

ACKNOWLEDGMENTS

This work is supported by the National 973 plan of China (No. G200003), the National Natural Science Foundation of China (Nos. 19775062 and 69976034) and the Shanghai Youth Foundation (No. 98JC14004).

[1] S. J. Pearton, J. W. Corbett, and M. Stavola, *Hydrogen in Crystalline Semiconductors* (Springer, Berlin, 1992), and references therein.
[2] *Hydrogen in Semiconductor*, edited by J. I. Pankove and N. M. Johnson (Academic, New York, 1990).
[3] *Defects in Semiconductors 17*, *Materials Science Forum*, edited by H. Heinrich and W. Jantsch (Trans-Tech, Switzerland, 1993), pp. 143–147.
[4] G. F. Cerofolini, R. Balboni, D. Bisero, F. Corni, S. Frabboni, G. Ottaviani, R. Tonini, R. S. Brusa, A. Zecca, M. Ceschini, G. Giebel, and L. Pavesi, Phys. Status Solidi A **150**, 539 (1995).
[5] J. Wong-Leung, C. E. Ascheron, and M. Petravic, Appl. Phys. Lett. **66**, 1231 (1995).
[6] J. Wong-Leung, E. Nygren, and J. S. Williams, Appl. Phys. Lett. **67**, 416 (1995).
[7] J. Wong-Leung, J. S. Williams, and R. G. Elliman *et al.*, Nucl. Instrum. Methods Phys. Res. B **96**, 253 (1995).
[8] M. Bruel, Electron. Lett. **31**, 1201 (1995).
[9] M. K. Weldon, V. E. Marsico, Y. J. Chabal, A. Agarwal, D. J. Eaglesham, J. Sapjeta, W. L. Brown, D. C. Jacobson, Y. Caudano, S. B. Christman, and E. E. Chaban, J. Vac. Sci. Technol. B **15**, 1065 (1997).
[10] A. Agarwal, T. E. Haynes, V. C. Venezia, O. W. Holland, and D. J. Eaglesham, Appl. Phys. Lett. **72**, 1086 (1998).
[11] G. F. Cerofolini, L. Meda, R. Balboni, F. Corni, S. Frabboni, G. Ottabviani, R. Tonini, M. Anderle, and R. Canteri, Phys. Rev. B **46**, 2061 (1992).
[12] R. S. Brusa, G. P. Karwasz, N. Tiengo, A. Zecca, F. Corni, G. Calzolari, and C. Nobili, J. Appl. Phys. **85**, 2390 (1999).
[13] R. S. Rrusa, M. Duarte Naia, A. Zecca, C. Nobili, G. Ottaviani, R. Tonini, and A. Dupasquier, Phys. Rev. B **49**, 7271 (1994).
[14] F. Corni, G. Calzolari, S. Frabboni, C. Nobili, G. Ottaviani, R. Tonini, G. F. Cerofolini, D. Leone, M. Servidori, R. S. Rrusa, G. P. Karwasz, N. Tiengo, and A. Zecca, J. Appl. Phys. **85**, 1401 (1999).
[15] D. Bisero, F. Corni, S. Frabboni, R. Tonini, G. Ottaviani, and R. Balboni, J. Appl. Phys. **83**, 4106 (1998).
[16] M. K. Weldon, (a) M. Collot, and Y. J. Chabal, V. C. Venezia, A. Agarwal, (b) T. E. Haynes, D. J. Eaglesham, S. B. Christman, and E. E. Chaban, Appl. Phys. Lett. **73**, 3721 (1998).
[17] C. M. Varma, Appl. Phys. Lett. **71**, 3519 (1997).